

Metallurgical and mechanical behavior of brazed thin alloys sheets assemblies

Elodie Martin¹, Jonathan Hugues², Eric Andrieu³, Jérôme Rocchi⁴

^{1,2,3}Université de Toulouse, Institut Carnot CIRIMAT, UPS/CNRS/INPT, ENSIACET, 4 allée Emile Monso, BP 44362, 31030 Toulouse Cedex 4

⁴Liebherr-Aerospace Toulouse SAS, 408 avenue des Etats-Unis, 31016 Toulouse Cedex 2

Abstract— Heat exchangers included in air conditioning systems for aircraft are produced by brazing stamped thin alloys sheets made of nickel-based alloys, Alloy 600 and Ni 201, or stainless steel, AISI 444. Separation metal sheets and locking bars of Alloy 625 are used to complete the system. The brazing filler metal, mainly composed of nickel, manganese, silicon and copper, is referred as BNi-8. In order to control brazing process, a good knowledge of both the brazing filler metal metallurgical behavior and of the interaction with the base metal is essential. The study of the brazing filler metal melting behavior in itself reveals that the melting point is highly dependent on the chemical composition and especially on silicon content. Microstructures analysis showed the presence of several phases with significant differences in terms of mechanical properties at a small scale which could induce local embrittlement. Interactions between the brazing filler metal and the different alloys constitutive of the assembly induce chemical composition evolutions related to the local configuration of the assembly. Dissolution and interdiffusion processes as well as chemical exchanges with the furnace environment occur. Finally, due to this set of phenomena, significant brazing defects can affect the mechanical integrity of the component.

Keywords— Brazing, Microstructure, Melting point, Nickel-based filler metal.

I. INTRODUCTION

Air to air heat exchangers assembled on aircraft are manufactured by brazing process. This joining process, carried out at high temperature and under controlled atmosphere, enables welding between different base metals due to brazing filler metal. During the brazing process, the temperature is chosen to be higher than the brazing filler metal liquidus but lower than the base metal solidus. According to Tuah-Poku et al. [1] and to J. Ruiz-Vargas et al. [2] most recently, brazing process could be divided in four steps: 1) melting of the filler metal, 2) widening of the liquid joint through dissolution of a part of the base metal, 3) isothermal solidification through diffusion from the liquid joint into the base metal and 4) final homogenization. During the second stage, the brazing filler metal wets base material surfaces, spreads along the joint between the base metals through capillary forces and diffuse into them [3] [4]. Finally, as explained in the last two steps, the joint is therefore made firstly by diffusion of the brazing filler metal in the base metal and secondly by solidification of residual liquid during the final cooling [5].

Air to air heat exchangers are complex structural components allowing to cool hot air collected from the engine by using cool air ducted from the engine fan. In the core of the pre-cooler, owing to an assembly of fluted thin metal sheets, interlayer plates and locking bars, heat transfers are optimized. To reduce the weight of component and optimize heat exchanges, thin metal sheets made of nickel-based alloys (Ni 201, Alloy 600 and Alloy 625) and ferritic stainless steel (AISI 444) are used as base metals together with a nickel-based brazing filler metal called BNi-8.

Brazing defects occur during the brazing cycle and can lead to a loss of mechanical integrity of the component. They are linked with the thermal cycle but also with the metallurgical transformations and deformations which the system is subjected to. To better understand the complex and multi-processes phenomena that occur during the brazing process, the metallurgical and mechanical behavior of the brazing filler metal and base metals were studied independently before focusing attention on the interaction between them. The aim of this multi-scale approach was to identify the first order microstructural variables controlling the macroscopic mechanical properties of the assembly.

II. MATERIALS AND METHODS

Three nickel-based metals (Ni 201, Alloy 600 and Alloy 625) and one ferritic stainless steel (AISI 444) were used. The chemical composition of Ni 201, Alloy 600, Alloy 625 and AISI 444 are given in the Table 1, Table 2, Table 3 and Table 4 respectively. The chemical composition of the brazing filler metal, produced by Wall Colmonoy Technologies, is given in the Table 5. Two batches were used in this study: A and B.

TABLE 1
CHEMICAL COMPOSITION OF NI 201 BASE METAL¹

Chemical composition (wt%)	C	Co	Cu	Fe	Mn	Ni	S	Si
Min	0	0	0	0	0	Bal.	0	0
Max	0.02	1.0	0.25	0.40	0.35		0.01	0.35

TABLE 2
CHEMICAL COMPOSITION OF ALLOY 600 BASE METAL¹

Chemical composition (wt%)	Al	C	Co	Cr	Cu	Fe	Mn
Min	0	0	0	14.0	0	6.0	0
Max	0.35	0.15	1.0	17.0	0.50	10.0	1.0
Chemical composition (wt%)	Nb	Ni	P	S	Si	Ta	Ti
Min	0	72.0	0	0	0	0	0
Max	1.0	80.0	0.04	0.015	0.50	0.05	0.50

TABLE 3
CHEMICAL COMPOSITION OF ALLOY 625 BASE METAL¹

Chemical composition (wt%)	Al	C	Co	Cr	Fe	Mn	Mo
Min	0	0	0	20.0	0	0	8.0
Max	0.40	0.10	1.0	23.0	5.0	0.50	10.0
Chemical composition (wt%)	Nb	Ni	P	S	Si	Ta	Ti
Min	3.15	58.0	0	0	0	0	0
Max	4.15	68.85	0.015	0.015	0.50	0.050	0.40

TABLE 4
CHEMICAL COMPOSITION OF AISI 444 BASE METAL¹

CHEMICAL COMPOSITION OF AISI 4145 STEEL						
Chemical composition (wt%)	C	Cr	Fe	Mn	Mo	N
Min	0.013	17.50	74.07	0	1.75	0
Max	0.025	19.50	80.49	1.0	2.50	0.035
Chemical composition (wt%)	Ni	P	S	Si	Ti (+Nb)	
Min	0	0	0	0	0.20	
Max	1.0	0.04	0.03	1.0	0.80	

TABLE 5
CHEMICAL COMPOSITION OF BNi-8 BRAZING FILLER METAL¹

CHEMICAL COMPOSITION OF BAY-BLANKET FILLER METAL						
Chemical composition (wt%)	Ni	Mn	Si	Cu	C	B
Min	Bal.	23.5	6.5	4.6	0	0
Max		24.9	7.2	5.4	0.1	0.1
Chemical composition (wt%)	O	N	P	C	Others (*)	
Min	0	0	0	0	0	
Max	0.05	0.05	0.02	0.1	0.5	

(*) S < 0.02 / Al < 0.05 / Ti < 0.05 / Zr < 0.05 / Co < 0.1 / Se < 0.005

¹ Internal technical sheet from Liebherr Aerospace Toulouse SAS
408 avenue des Etats-Unis
31016 Toulouse Cedex France

Optical Microscopy (OM) and Scanning Electron Microscopy (SEM) were used to characterize the microstructures. Microstructural evolution of the base metal between the as-received state and after brazing cycle was characterized by using Electron BackScatter Diffraction (EBSD). The SEM used was a FEG-SEM JEOL JSM 7000F equipped with a Schottky field emission source. The EBSD camera was coupled to the software Channel 5 Oxford Instruments for data processing. As an excellent surface preparation is necessary for these samples, the specimens of 10 mm x 10 mm were cut out and polished electrochemically with the A2 solution from Buelher under electrochemical conditions (V, t, T) adapted to the studied material. This surface preparation helps to relieve residual stresses that could be created during the sample preparation. Samples are tilted at 70° and the tilt axis is parallel to the L-LT rolling axis of the metal sheet. In these operating conditions, an indexation rate above 99 % was reached.

The chemical composition of the different phases was measured by using Energy Dispersive X-ray Spectrometry (EDX) and Electron Probe MicroAnalysis (EPMA). The EPMA was a CAMECA SXFive. The acceleration voltage of the electron gun, equipped with a tungsten filament, was fixed at 15 kV and the beam current applied to 20 nA so that the analyzed corresponding material volume was close to a few μm^3 . In the present study, alloying elements of interest were: nickel, chromium, manganese, niobium, molybdenum, iron, silicon and copper.

Mechanical properties were measured as a result of tensile tests with a MTS Criterion Model 43 equipped with self-tightening grips, load system of 5 kN and a high-temperature extensometer. The tests were carried out at room temperature as follows: load up to 20 N, 10 seconds hold, load up to fracture under displacement rate control at 0.02 mm/s.

III. RESULTS AND DISCUSSION

3.1. Brazing filler metal

The brazing filler metal microstructure was studied for two different batches (A and B) after brazing cycle. In order to avoid the industrial furnace atmosphere effects, the small ingots were molten into quartz tubes which were sealed under vacuum at room temperature.

As one can see on Fig. 1, microstructural heterogeneities in two batches are evidenced.



FIG. 1. OPTICAL MICROGRAPHS SHOWING MICROSTRUCTURES OBTAINED AFTER THE BRAZING CYCLE FOR BATCH A (LEFT) AND BATCH B (RIGHT)

As expected, Batch A is composed of an eutectic microstructure with large unexpected blocky crystals, particularly near the periphery of the ingot. On the contrary, Batch B shows a dendritic solidification structure without large crystals. To better understand these microstructural differences, chemical analyses were carried out. The average chemical composition for the crystal and the dendritic phases are given in the Table 6.

TABLE 6

AVERAGE CHEMICAL COMPOSITION FOR THE CRYSTAL AND THE DENDRITIC PHASES (EPMA ANALYSES)

Chemical composition (wt%)	Ni	Mn	Si	Cu
Crystal phases	67.2 ± 0.4	24.5 ± 0.2	12.6 ± 0.3	0.8 ± 0.1
Dendritic phases	65.4 ± 0.2	22.2 ± 0.1	2.6 ± 0.1	6.8 ± 0.3

From these analyses, it was concluded that silicon was identified as responsible of these microstructural evolutions. In fact, the silicon content varies from 7.5 wt (%) for Batch A to 5.9 wt (%) for batch B at the as-received state. Finally, for the silicon-rich batch and the silicon-poor batch, an eutectic structure with large crystals rich in silicon and an eutectic structure

with primary dendrites of solidification respectively, were obtained. However, for the two batches, a terminal eutectic with a very fine structure as shown on the Fig. 2 was found.

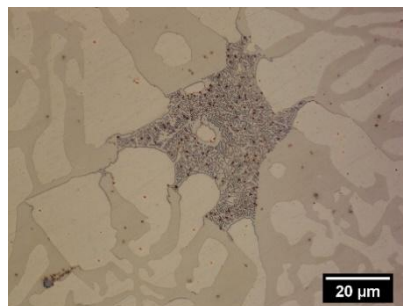


FIG. 2 OPTICAL MICROGRAPH SHOWING A TERMINAL EUTECTIC FOR THE BATCH B

3.2. Base metals

The metallurgical and mechanical evolutions of base metals were characterized as a function of temperature. Given the thickness of the base metal sheet, 50 microns for Ni 201, Alloy 600 and AISI 444, changes in grain size between the as-received state and after the brazing cycle were studied by EBSD. The grain size evolutions are presented on the Fig. 3.

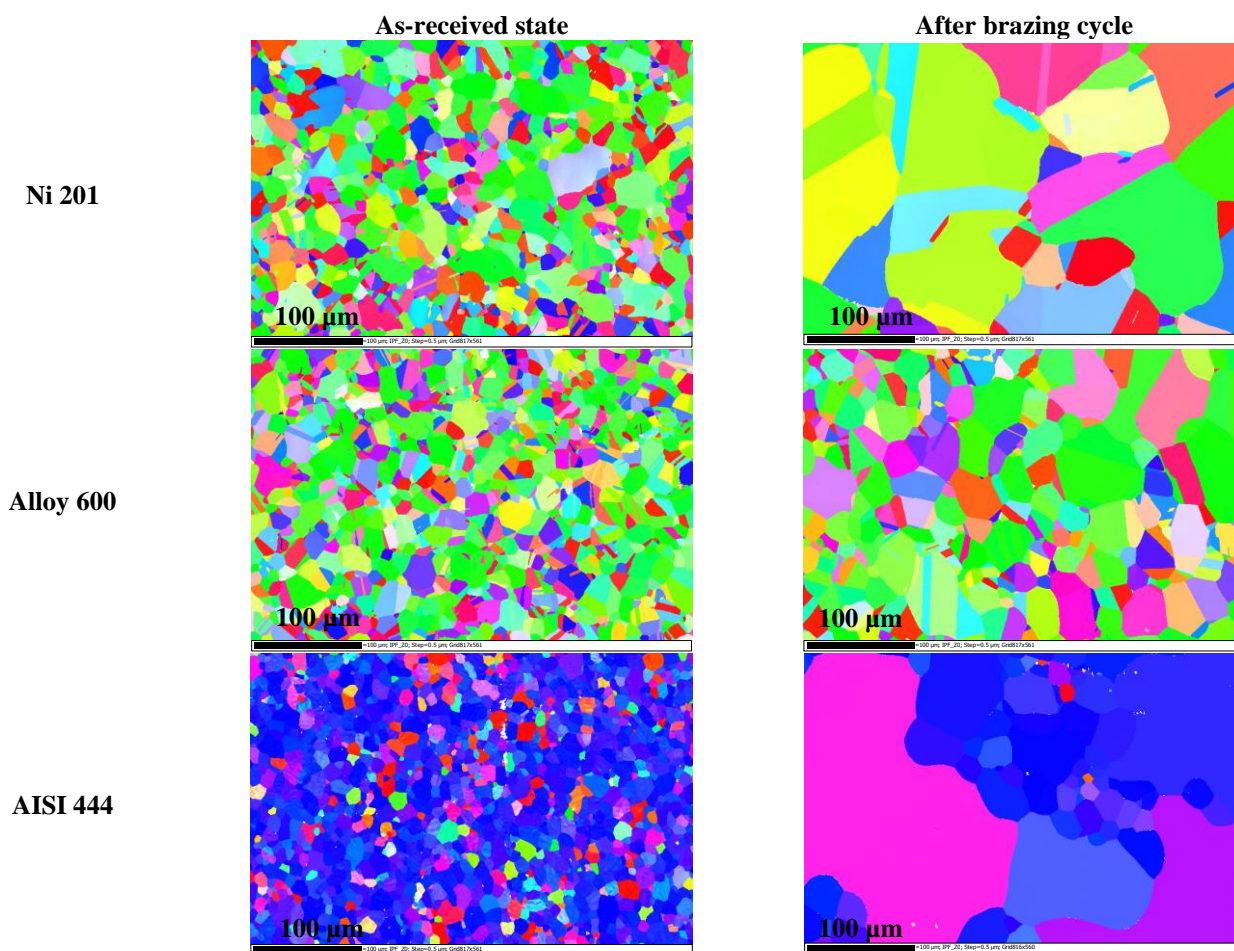

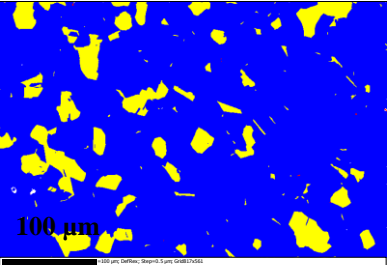
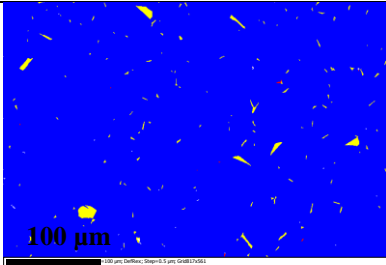
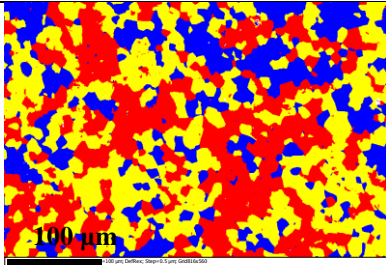


FIG. 3 EBSD MAPPINGS AT THE AS-RECEIVED STATE (LEFT) AND AFTER BRAZING CYCLE (RIGHT)

The applied brazing cycle induced a significant grain growth: the average grain size increased from 15 microns for the two nickel based metals up to approximately 100 microns and 25 microns for the Ni 201 and for the Alloy 600 after the brazing cycle, respectively. Concerning, the ferritic stainless steel, the as-received grain size was about 10 microns and reached 30 microns in average after the brazing cycle. However, as Fig. 3 shows, the grain size evolution appears very heterogeneous from 1.8 μm to 187.6 μm . By comparing the average grain size of the final grains with the thickness of the metal sheet, it is worth mentioning that in most of the cases, there are one or two grains in the thickness of the sheet. In terms of microstructure these sheets could be compared to plane (2D) polycrystal which usually did not behave as volume (3D) polycrystal.

Given that the Ni 201 contains a few alloying elements, the grain growth is easier. Due to pinning of grain boundaries by $M_{23}C_6$ carbides intergranular precipitation, the grain growth in Alloy 600 seems to be limited [6]. Meanwhile, the AISI 444 shows a heterogeneous growth of the grains. In order to investigate a possible occurrence of recrystallization during the brazing heat treatment, misorientation mappings were carried out on as-received thin sheets (see Table 7).

TABLE 7
MISORIENTATION MAPPINGS IN THE BASE METALS AT THE AS-RECEIVED STATE

Ni 201	Alloy 600	AISI 444
 <p>Recrystallized fraction Substructured fraction Deformed fraction</p>		
		
Recrystallized: 84.8 % Sub-structured: 15.1 % Deformed: 0.1%	Recrystallized: 98.8 % Sub-structured: 1.1 % Deformed: 0.1%	Recrystallized: 23.7 % Sub-structured: 40.6 % Deformed: 35.7%

For nickel based alloys, a majority of recrystallized grains seemed to be evidenced. For this alloys family, the initial stored mechanical energy is so low that solely grain growth is likely to occur during the brazing treatment. In the case of AISI 444, in addition to the recrystallized and substructured grains, a considerable amount of deformed grains was observed. Consequently, mechanical energy stored in the polycrystal is large and recrystallization processes could occur during the brazing heat treatment. The qualitative diagram, Fig. 4, indicates that resultant grain size depends on deformation rate and annealing temperature. Indeed, for low deformation rates, the higher the annealing temperature, the larger the grains will become. On the contrary, for large deformation rates and whatever any annealing temperature, the obtained grains will be small.

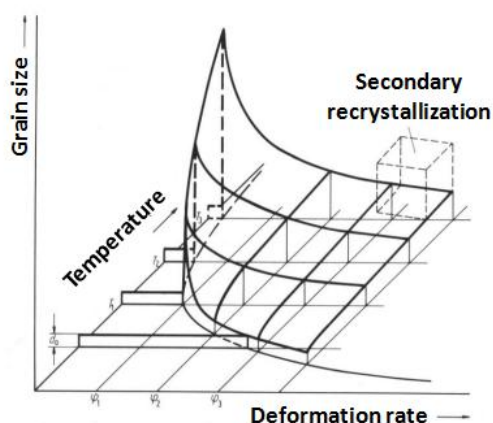


FIG. 4 RECRYSTALLIZATION DIAGRAM ADAPTED FROM [7]

Thus, for the initial grains which are recrystallized, the amount of energy stored does not exceed the critical value allowing the germination phenomenon. As a consequence, the grains grow. This is the observed phenomena in the case of nickel based alloys, Ni 201 and Alloy 600. On the contrary, for deformed grains where the stored energy is greater, nucleation of new grains is favored and small grains are obtained. This is probably the reason why, after the brazing heat treatment, the AISI 444 presents a heterogeneous microstructure with large grains and small grains respectively due to the initially recrystallized and initially deformed grains.

In order to understand the effect of microstructural evolution on the mechanical properties, tensile tests were carried out at room temperature. The base metal sheets were tested at the as-received state and after been exposed to a brazing cycle in the industrial furnace to determine the influence of the heat treating temperature on the mechanical behavior. The conventional yield strength (YS in MPa), the ultimate tensile strength (UTS in MPa) and the elongation at fracture (ϵ_R in %) are given in the Table 8 for Ni 201, Alloy 600 and AISI 444. All the fractures surfaces were ductile with dimples.

TABLE 8
BASE METALS MECHANICAL PROPERTIES AT THE AS-RECEIVED STATE AND AFTER BRAZING CYCLE IN THE INDUSTRIAL FURNACE

Base metals	Ni 201		Alloy 600		AISI 444	
Conditions	As-received state	After brazing cycle	As-received state	After brazing cycle	As-received state	After brazing cycle
YS (MPa)	184	83	312	200	375	284
UTS (MPa)	449	303	802	551	710	419
ϵ_R (%)	14	11	19	16	22	10
Fractures surfaces	Ductile		Ductile		Ductile	

Evolutions of the mechanical behavior of the three base metals are quite similar. Indeed, the conventional yield strength (YS), the ultimate tensile strength (UTS) and the elongation at fracture (ϵ_R) are higher at the as-received state in comparison to the brazed state. Concerning the elongation at fracture (ϵ_R), AISI 444 seems to be more sensitive to the brazing treatment than Ni 201 and Alloy 600. The modifications of the mechanical properties can be associated with the metallurgical modifications of the base metals and in particular the increase of the average grains size.

E. Hall and N. Petch [8] [9] showed that when the grain size is greater than a few hundred microns, a decrease in grain size leads to an overall strengthening. P. Janssen et al. [10] demonstrated that when the grain size is less than a few microns, the effect of the grain size is reduced. Furthermore, C. Keller and E. Hug [11] have shown that a decrease in the number of grain in the thickness of the sample below a critical value decreases the flow stress. This experimental fact might be rather problematic when dealing with dimensional stability of brazed structures.

3.3. Interactions between base metals and brazing filler metal

In order to evaluate the interactions between base metals and brazing filler metal, materials assemblies were produced as it is shown on the following scheme, Fig. 5:

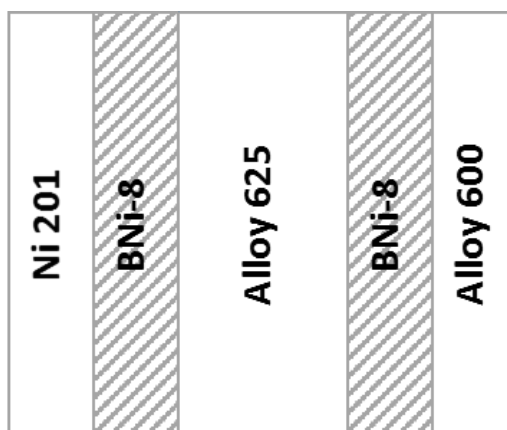


FIG. 5. ASSEMBLIES SCHEMATIC DIAGRAM

All assemblies underwent a brazing cycle in the industrial furnace: Ni 201/BNi-8/Alloy 625/BNi-8/Alloy 600, Alloy 600/BNi-8/Alloy 625/BNi-8/AISI 444 and AISI 444/BNi-8/Alloy 625/BNi-8/Ni 201. Results for the Ni 201/BNi-8/Alloy 625/BNi-8/Alloy 600 system are presented in this paper. The metallurgical state of the different interfaces were first characterized by using backscattered electrons imaging, Fig. 6.

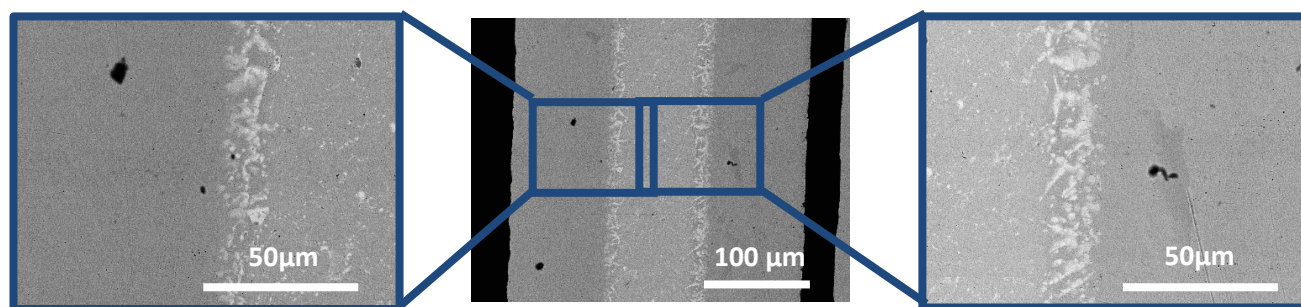


FIG. 6 SEM IMAGES IN BACKSCATTERED ELECTRONS FOR Ni 201/BNi-8/ALLOY 625/BNi-8/ALLOY 600 SYSTEM

An analysis profile made with the EPMA is presented on the Fig. 7. On the ordinate scales (left and right), the chemical composition of the various elements is given in weight percent (wt%). On the abscissa scale, the length is given in μm . The vertical dotted lines represent approximately the final interfaces determined arbitrarily by the chemical composition profiles of the different elements. The initial thicknesses of the base metals are then reduced in favor of the widening of the joint. Indeed, the base metals are partially dissolved in the brazing filler metal during the brazing process. The tight and wide dotted lines respectively separate the metal sheets (Ni 201 and Alloy 600) from the brazing filler metal (BNi-8) and the separating plate (Alloy 625) from the brazing filler metal.

On the two ordinates axes, the initial quantity of alloying elements is represented by a symbol and a specific color for each of the materials. The chemical elements contained in Ni 201 are represented by a blue square, those in Alloy 600 by an orange diamond, those in Alloy 625 by a yellow triangle and those in BNi-8 by a green cross. Only the chemical compositions of the main elements are represented. The chemical composition of the elements inscribed in the legend on the left is read on the left ordinate (principal axis) and that of those inscribed in the legend on the right is read on the right ordinate (secondary axis).

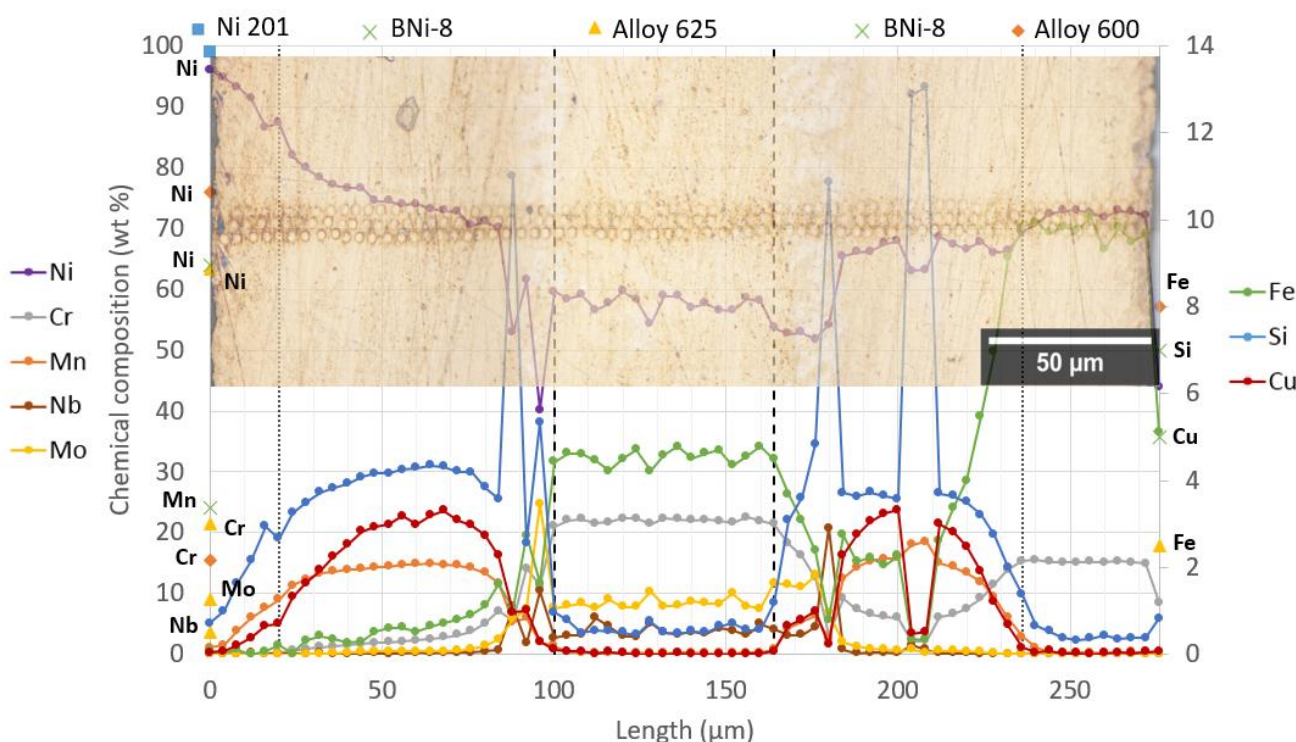


FIG. 7 CHEMICAL COMPOSITION PROFILES FOR NI 201/BNi-8/ALLOY 625/BNi-8/ALLOY 600 SYSTEM (EPMA)

The interdiffusion of the elements (manganese, silicon, molybdenum, niobium and chromium), between the brazing filler metal and the base metal, induces precipitation with chemical composition gradients.

Two populations of precipitates are present:

- The first family of precipitates, located on each side of the Alloy 625 sheet, is due to the strong interactions between the metal sheet and the brazing filler metal, Fig. 6, Fig. 7, Fig. 8 and Fig. 10

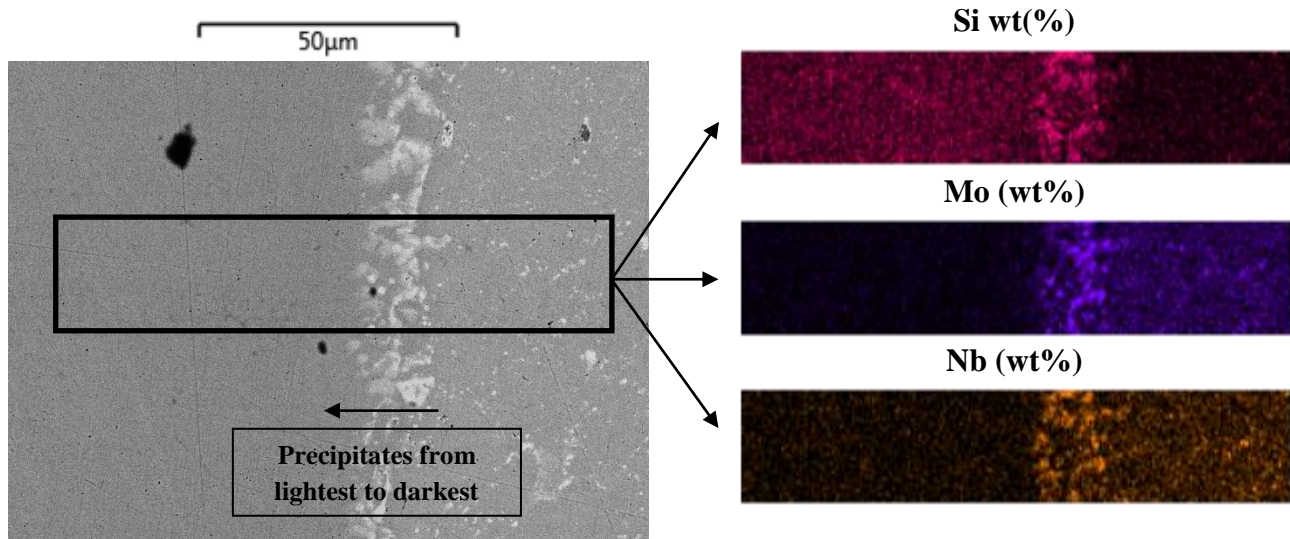


FIG. 9 EDX RESULTS FOR Ni 201/BNi-8/ALLOY 625 INTERFACE

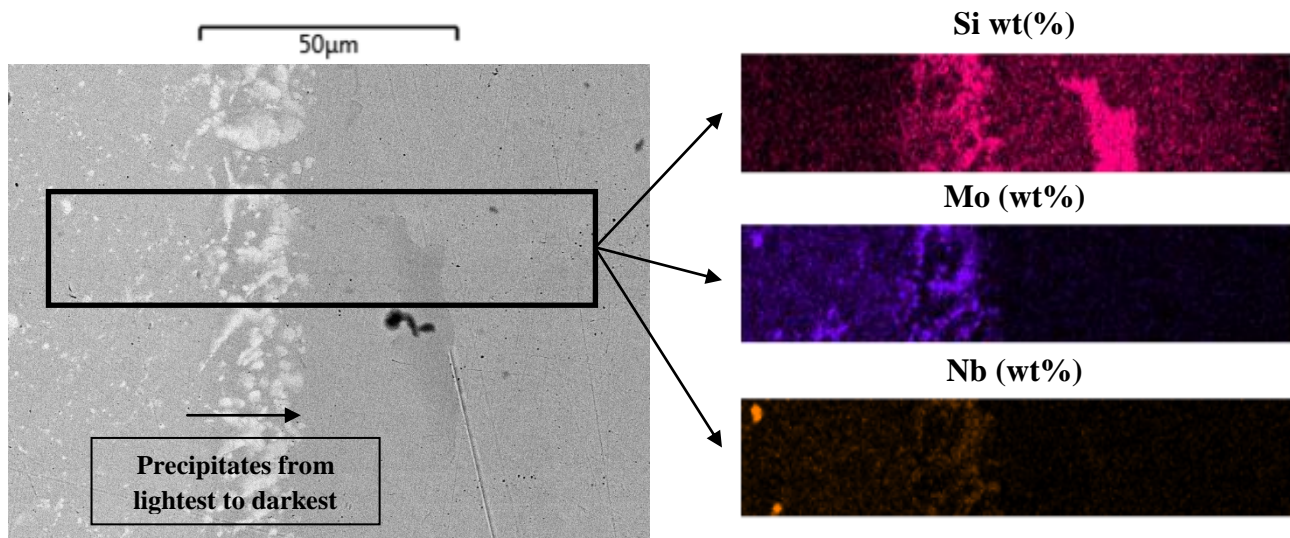


FIG. 10 EDX RESULTS FOR ALLOY 625/BNi-8/ALLOY 600 INTERFACE

These precipitates have a color gradient in backscattered electrons imaging, lighter on the side of the Alloy 625 sheet and darker on the side of the brazing filler metal.

The chemical composition for the light and dark precipitates is given in the Table 9.

TABLE 9
PRECIPITATES COMPOSITION IN BNi-8/ALLOY 625 INTERFACE (EPMA)

Chemical composition (wt%)	Ni	Cr	Mo	Nb	Si
Light precipitates	30.3-43.6	6.5-12.0	21.8-35.3	4.2-14.8	6.2-8.7
Dark precipitates	55.6-60.2	2.0-7.2	5.2-7.4	10.3-19.3	7.5-12.0

One can notice that the chromium content is smaller in the dark precipitates. This observation seems to be logical because the chromium source for interdiffusion process is the Alloy 625. Moreover, it is worth noting that the niobium content is very large, which suggests that this element diffuses faster from the base metal to the brazing filler metal as compared to the molybdenum for example. In addition, as the molybdenum has an atomic number (Z) greater than niobium, it is expected that the precipitates richer in molybdenum, close to the Alloy 625 sheet, appears brighter.

- The second family of precipitates appears as discontinuous dark bands in backscattered electrons imaging in the brazing filler metal, Fig. 6 on the right, Fig. 7 and Fig. 10. The analysis of these phases reveals that they are rich in manganese (15.2-18.6 wt%) and in silicon (12.5-12.8 wt%), the remainder mainly completed with nickel. These phases must correspond to the last portion of liquid that has solidified to the eutectic composition. The proportion of silicon-rich phase seems greater compared to that rich in copper. These hard eutectics phases constitute a fragile zone.

In the case of AISI 444 association, we also find another type of precipitates at the brazing filler metal core. These lighter, rounded-shaped precipitates are rich in manganese (7.3-15.2 wt%), in silicon (11.9-12.5 wt%) and contain a small amount of niobium (3.6-13.8 wt%) and molybdenum (3.0-6.7 wt%), the rest being supplemented by nickel, as before. The molybdenum and niobium presence gives brighter precipitates in backscattered electrons imaging as explained above.

According to the analyses with EPMA, the interactions on both sides of the Alloy 625 sheet are symmetrical and do not seem to be influenced by the base metal on the other side of the brazing filler metal. The scale of the interaction zone is therefore limited. However, the interactions between the base metal (Ni 201, Alloy 600 and AISI 444) and the brazing filler metal (BNi-8) are dependent on the base metal. Indeed, the precipitation between the Ni 201 and the brazing filler metal for example is less complex than that with Alloy 600 and with AISI 444. The interdiffusion phenomena are more complicated for highly alloyed base metals.

The mechanical strength of the different assemblies has also been tested at room temperature. As a matter of example, the fracture surfaces at different locations for the Ni 201/BNi-8/Alloy 625/BNi-8/Alloy 600 system are shown on the Fig. 11. On the right and left fractographs, Ni 201 is at the top of the pictures, Alloy 625 in the center and Alloy 600 in the bottom. The central fractograph shows the ductile fracture surface outside and in the center of the assembly. At the interface, the fracture surface appears intergranular ductile with large porosities where powder grains are visible.

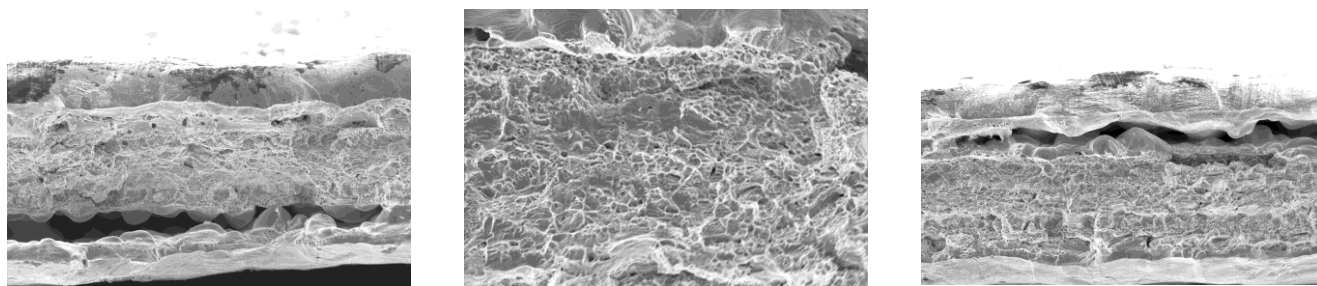


FIG. 11 SEM IMAGES IN SECONDARY ELECTRONS FOR Ni 201/BNi-8/ALLOY 625/BNi-8/ALLOY 600 SYSTEM

The global mechanical properties for the three assemblies are given in Table 10.

TABLE 10
MECHANICAL PROPERTIES FOR THE BASE METAL ASSEMBLIES

Base metal assemblies	Ni 201/BNi-8/Alloy 625/BNi-8/Alloy 600	Ni 201/BNi-8/Alloy 625/BNi-8/AISI 444	Alloy 600/BNi-8/Alloy 625/BNi-8/AISI 444
YS (MPa)	317	259	348
UTS (MPa)	543	355	494
ϵ_R (%)	8	4	5

According to the results, the Ni 201/BNi-8/Alloy 625/BNi-8/AISI 444 system is the worst association. On the assembly microstructure, a continuous line of very hard silicon-rich phases, which could be at the origin of the premature fracture, is observed. The Alloy 600/BNi-8/Alloy 625/BNi-8/AISI 444 system has the best yield strength (YS). Finally, the Ni 201/BNi-8/Alloy 625/BNi-8/Alloy 600 system seems to be the best compromise with the best ultimate tensile strength (UTS) and the best elongation at fracture (ϵ_R).

Owing to fracture surfaces analysis, one can see that the damage is located in the joint. However, detail analyses have to be performed to identify the damaging mechanism. Indeed, two hypotheses can be proposed to explain the fracture surface morphology. The first hypothesis suggests that the fracture initiation occurred in the joint because of the growth of already existing porosities due to solidification process of a thin film of liquid alloy. The second one deals with a premature fracture initiation due to the decohesion of the silicon-rich eutectics phases thus initiating a cavity that grows plastically until it breaks. The silicon-rich eutectics phases present in the brazing filler metal are very hard and equivalent to inclusions that do

not deform and prefer to break suddenly. When these eutectics phases are distributed discontinuously, the succession of "hard" and "soft" phases can be responsible for the formation of a kind of broken dotted line.

Other tests intended to get information dealing with dimensional instabilities during brazing cycle were carried out on brazing filler metal-coated thin sheets. Brazing filler metal discs were deposited on the different base metals. The supports were 100 mm squares covered with a mask with a 30 mm diameter window in the center. The brazing filler metal was then deposited only in the window. It was given to this type of sample a brazing cycle. Following this treatment, the topography of the sample was measured using an optical 3D profilometer (Alicona). The profile for the BNi-8/Ni 201 system is presented on the Fig. 12.

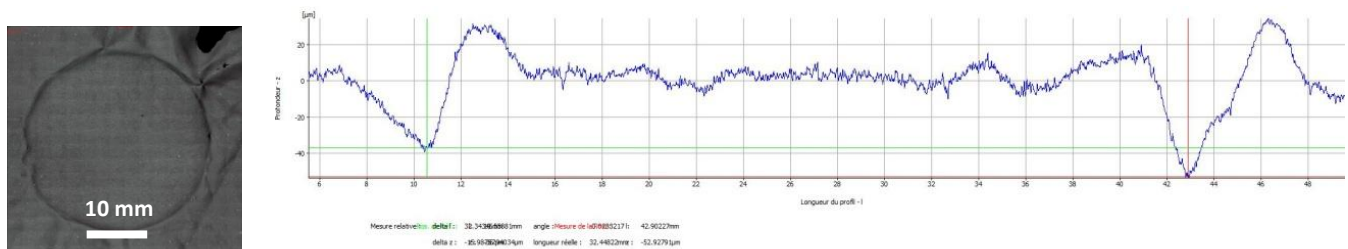


FIG. 12 IMAGES AND PROFILES ACCORDING TO THE DIAMETER OF THE BRAZING FILLER METAL DISC FOR THE BNi-8/Ni 201 SYSTEM

In order to evaluate the geometrical consequences of brazing process, the ratio between the lengths of the reference profile and the real profile is calculated. The length of the reference profile corresponds to the brazing filler metal disc diameter while that associated with the real profile corresponds to the developed length. An isotropic deformation of the order of 1 %, corresponding to an expansion of the disc of coated with brazing filler metal, was found. By relating this percentage to the standard length of a heat exchanger, namely 300 mm, the expected displacements then of the order of 3 mm. Thus, significant dimensional instability can be observed. Assuming that it occurred during the solidification of the brazing filler metal because of the phase transformations which leads to a volume expansion. Moreover, a difference of thermal expansion coefficient could also contribute to this type of effect.

IV. CONCLUSION

Before studying the interactions between base metals and brazing filler metal, it has been observed that small variations of chemical composition induce different solidification paths and thus different microstructures and mechanical behavior. For base metals, it has been seen that brazing conditions in terms of temperature had an effect on the microstructure and hence on the mechanical properties. The brazing cycle induces a decrease in mechanical strength. Finally, for the assemblies, the precipitates formed in the interaction zone between the brazing filler metal and the metal sheets seems to play a first order role in the final mechanical response of the assembly. Nevertheless, precipitation is also present in the core of the brazing filler metal. When precipitates are in a continuous eutectic form, the mechanical strength is greatly reduced. It is therefore essential to define selection criteria in terms of brazing filler metal chemical composition and thickness of the deposit to optimize the mechanical behavior of the considered assemblies.

REFERENCES

- [1] I. Tuah-Poku, M. Dollar, and T. B. Massalski. A study of the transient liquid phase bonding process applied to a Ag/Cu/Ag sandwich joint. *Metallurgical Transactions A*, 19(A):675–686, 1988.
- [2] J. Ruiz-Vargas, N. Siredey-Schwaller, P. Bocher, and A. Hazotte. First melting stages during isothermal brazing, of Ni/BNi-2 couples. *Journal of Materials Processing Technology*, 213(12):2074 – 2080, 2013.
- [3] I. Amato, F. Baudrocco, and M. Ravizza. Spreading and aggressive effects by nickel-base brazing filler metals on the alloy 718. *Welding research supplement*, 1972.
- [4] X. P. Zhang and Y. W. Shi. A dissolution model of base metal in liquid brazing filler metal during high temperature brazing. *Scripta Materialia*, 50, 2004.
- [5] S. K. Tung, L. C. Lim, and M. O. Lai. Solidification phenomena in nickel base brazes containing boron and silicon. *Scripta Materialia*, 34(5):763–769, 1996.
- [6] H. Tézenas Du Montcel. Ingénierie des joints de grains dans les superalliages à base de nickel. PhD thesis, Ecole doctorale n°432 : Sciences et génie des matériaux, 2012.
- [7] H. J. Bargel and G. Schulze. *Werkstoffkunde*. 5ème edition, 1988.

-
- [8] E. O. Hall. The deformation and ageing of mild steel: III Discussion of results. *Physical Society of London*, 64:p. 747–753, 1951.
- [9] N. J. Petch. The cleavage strength of polycrystals. *Journal of the Iron Steel Institute* 174, 1953.
- [10] P. J. M. Janssen, Th. H. de Keijser, and M. G. D. Geers. An experimental assessment of grain size effects in the uniaxial straining of thin Al sheet with a few grains across the thickness. *Materials Science & Engineering*, A(419):238–248, 2006.
- [11] C. Keller and E. Hug. Hall-Petch behaviour of Ni polycrystals with a few grains per thickness. *Materials letters*, 62:1718–1720, 2008.